The Quaternary Structure of the HisZ−HisG *N*-1-(5′-Phosphoribosyl)-ATP Transferase from *Lactococcus lactis*†

Michael L. Bovee,‡ Karen S. Champagne,‡ Borries Demeler,§ and Christopher S. Francklyn*,‡

Department of Biochemistry, The University of Vermont Health Sciences Complex, Burlington, Vermont, 05405-0068, and Department of Biochemistry, MSC 7760, The University of Texas Health Science Center at San Antonio, 7703 Floyd Curl Drive, San Antonio, Texas 78229-3900

Received March 27, 2002; Revised Manuscript Received July 11, 2002

ABSTRACT: The *N*-1-(5′-phosphoribosyl)-ATP transferase (ATP−PRTase) encoded by the *hisG* locus catalyzes the condensation of ATP with PRPP, the first reaction in the biosynthesis of histidine. Unlike the homohexameric forms of the enzyme found in *Escherichia coli* and *Salmonella typhimurium*, the ATP−PRTase from *Lactococcus lactis* and a number of other bacterial species consists of two different polypeptides, both of which are required for catalytic activity (Sissler et al. (1999) *Proc. Natl. Acad. Sci. 96*, 8985−8990). The first of these is a truncated version of HisG that is approximately 100 amino acids shorter than the canonical versions. The second, HisZ, is a 328-residue version of a class II aminoacyl-tRNA synthetase catalytic domain that possesses no aminoacylation function. Here, the molecular mass and subunit composition of the *L. lactis* HisZ−HisG heteromeric ATP−PRTase is investigated using liquid chromatography, analytical ultracentrifugation, and quantitative protein sequencing. Individually, HisZ and HisG form inactive but stable dimers with association constants in the range of $2.5-3.3 \times 10^5$ M^{-1}. When both types of subunits are present, a quaternary octamer complex is formed with a sedimentation coefficient of 10.1 S. Incubation of this complex with ATP promotes a shift to 10.7 S. By contrast, incubation with the allosteric modulators AMP and histidine destabilizes the complex, resulting in a shift to multiple species in equilibrium with an average of 9.3 S. While this octameric structure is unique to both the phosphoribosyl transferases and the aminoacyl-tRNA synthetases, the change in sedimentation behavior elicited by substrates and inhibitors suggests the presence of allosteric regulatory mechanisms reminiscent of other multisubunit enzymes of metabolic importance.

The first step in the biosynthesis of histidine consists of the condensation of *N*-1-(5′-phosphoribosyl) pyrophosphate (PRPP)[1] with ATP, a reaction catalyzed by *N*-1-(5′-phosphoribosyl)-adenosine triphosphate phosphoribosyltransferase (ATP-PRTase; EC 2.4.2.17) (*1*). In the Gram-negative prokaryotes *Salmonella typhimurium* and *Escherichia coli*, ATP-PRTase is encoded by the first gene in the *his* operon, *hisG* (*2*). Under standard physiological conditions, the ATP-PRTases from these prokaryotes are homooligomers composed six polypeptide chains of 299 residues (*3*, *4*). Interest in HisG arises from its catalysis of the first committed step of histidine biosynthesis, which is highly regulated. The primary regulation of the pathway is feedback inhibition of HisG by histidine, but the levels of the histidine biosynthetic enzymes are also regulated via a complex mechanism involving attenuation (*5*, *6*). In addition to feedback regulation by histidine, HisG is further regulated by adenine nucleotides and ppGpp. Owing to its presence in bacteria, fungi, and plants and its absence in mammals, the histidine biosynthetic pathway has been the target of various inhibitors, particularly herbicides (*7*).

Recently, a new form of ATP-PRTase was reported (*8*). Unlike the homomeric ATP-PRTases of *S. typhimurium* and *E. coli*, the ATP-PRTase from Gram-positive *L. lactis* is heteromeric, comprised of two distinct polypeptides (*8*). The first of these is a shorter form of HisG that is missing about 100 residues from its C-terminal end and exhibits no ATP-PRTase function on its own. To reconstitute a functional ATP-PRTase, the short form of HisG associates noncovalently with a second polypeptide, HisZ, that is 25% identical to the catalytic domain of histidyl-tRNA synthetases. In the genomes of *L. lactis* and *Bacillus subtilis*, the *hisZ* and *hisG* genes are adjacent to each other in the histidine biosynthetic operon (*9*, *10*). HisZ contains all three of the peptide motifs diagnostic for the class II tRNA synthetases (*11*) but possesses neither aminoacylation or ATP-PRTase function (*8*). Phylogenetic analysis also indicates that HisZ forms a clade distinct from the functional histidyl tRNA synthetases and probably diverged from them early in the evolution of the bacteria (*12*). Although the presence of HisZ is clearly required to convert the short form

† This work was supported by Grants GM54899, GM19739, and DOE-EPSCOR. UltraScan software development was supported by NSF Grant DBI-9974819 to B.D.

* To whom correspondence should be addressed. Phone: (802) 656-8450. Fax: (802) 862-8229. E-mail: cfranckl@zoo.uvm.edu.

‡ The University of Vermont Health Sciences Complex.

§ The University of Texas Health Science Center at San Antonio.

[1] Abbreviations: ATP, adenosine triphosphate; PRPP, *N*-1-(5′-phosphoribosyl)pyrophosphate; PR−ATP, *N*-1-(5′-phosphoribosyl)-ATP; ATP−PRTase, *N*-1-(5′-phosphoribosyl)-ATP phosphoribosyl transferase; SEC, size exclusion chromatography; SEC-LS, liquid chromatography light scattering; *S*, Svedberg sedimentation constant corrected to pure water at 20 °C ($S^0_{20,w}$).

10.1021/bi020243z CCC: $22.00
Published on Web 08/31/2002

of HisG to an active ATP-PRTase, its precise function in the complex is unclear.

The PRTases include at least three structurally distinct families, each of which is characterized by a unique catalytic domain architecture (*13*−*15*). The largest of these is the type I subfamily, whose members are distinguished by a Rossman nucleotide binding fold in their catalytic domains (*13*). These also share a characteristic signature sequence associated with binding PRPP. The absence of this signature sequence in HisG and the low extent of sequence identity between HisG and other PRTases suggest that it might possess a fold not yet observed in other PRTases. In the absence of detailed structural information obtainable by crystallography or other high resolution approaches, early biochemical work on HisG focused on the relationship of oligomeric structure to catalytic function and regulation (*3*, *4*).

Despite these efforts, the impact of structure on HisG function is poorly understood, and different subunit stoichiometries have been proposed for the active forms of the ATP-PRTases from *S. typhimurium* and *E. coli* (*16*). Both enzymes also appear to respond in different ways to changes in pH, temperature, and other solution conditions. However, the *E. coli* and *S. typhimurium* HisG polypeptides are both 299 residues in length, and the sequences are 90% identical. On the basis of this strong similarity, it seems unlikely that the active forms of the two proteins would have different quaternary structures. Here, the quaternary structures of the HisZG heteromeric ATP-PRTase from *L. lactis* and its HisZ and HisG constituents are addressed using chromatographic and hydrodynamic methods. These studies indicate that the isolated HisZ and HisG proteins are best described by simple monomer−dimer models, while the HisZG ATP-PRTase is best described as an octamer composed of four subunits each of HisZ and HisG. The sedimentation properties of the complex also vary according to the substrates or inhibitors that are present. The implications of these results for the evolution and function of the ATP-PRTases are discussed.

EXPERIMENTAL PROCEDURES

Reagents and Buffers. Reagent-grade chemicals and deionized glass distilled water were used in the preparation of all buffers and solutions. Unless otherwise noted, all chemicals and biochemical reagents were purchased from Fisher Scientific or Sigma. Buffers for the purification of *L. lactis* HisZ, *B. subtilis* HisG, and *L. lactis* HisZG included the following: wash buffer (WB; 50 mM sodium phosphate pH 7.5, 300 mM KCl, 10% glycerol, 10 mM β-mercaptoethanol); hydroxyapatite buffer A (HA; 50 mM potassium phosphate pH 7.0, 100 mM KCl, 10 mM β-mercaptoethanol) and hydroxyapatite buffer B (HB; 1 M potassium phosphate pH 7.0, 100 mM KCl, 10 mM β-mercaptoethanol). Analytical ultracentrifugation experiments were carried out in buffer AUB (50 mM sodium phosphate, pH 7.5, 150 mM sodium chloride, 10 mM $MgCl_2$, 3 mM β-mercaptoethanol) or AUB plus the following ligands: 1 mM ATP, 0.2 mM PRPP, 1 mM histidine, or 0.75 mM AMP.

Protein Purifications. The HisZ−HisG complex and isolated HisZ and HisG components were all produced from *E. coli* overexpression strains by modifications of the protocol described previously (*8*). In the pMS-100 expression construct used for the expression of the *L. lactis* HisZ−HisG ATP-PRTase complex, the His_6-tagged *hisZ* open reading frame and that of *hisG* are arranged in tandem as they are in the genomic sequence, such that the two coding regions overlap by two codons (*9*). This results in reduced expression of HisG relative to HisZ. By virtue of the hexahistidine (His_6) affinity tag on HisZ and the noncovalent association between coexpressed HisZ and HisG, the two proteins copurify as a complex (*8*) along with excess tagged HisZ on Ni−NTA agarose (Qiagen). Consequently, the purification protocol was augmented for separation of the HisZG ATP-PRTase complex from free (and presumably uncomplexed) HisZ as described below. Independently expressed HisZ from *L. lactis* and HisG from *B. subtilis* were purified using Ni−NTA agarose chromatography (*8*).

To ensure separation of the HisZG complex from traces of free HisZ, fractions from the Ni−NTA chromatography step that contained both HisZ and HisZG were pooled and then dialyzed against wash buffer (WB; 50 mM sodium phosphate pH 7.5, 300 mM KCl, 10% glycerol, 10 mM β-mercaptoethanol) to remove imidazole. After concentration, the Ni−NTA fractions were applied to a Superdex 200 (Pharmacia) sizing column preequilibrated in WB. Size exclusion chromatography was performed under isocratic conditions in buffer WB, and then samples containing protein were identified by absorbance at 280 nm and analysis by SDS−PAGE. Additional purification of the HisZ−HisG complex was achieved by fractionating pooled material from the Superdex 200 peak on a HA Ultrogel hydroxyapatite column (BioRad). Separation of the HisZG complex from HisZ was accomplished with a gradient of buffers HA and HB. Fractions containing HisZG were detected by absorbance at 280 nm and SDS−polyacrylamide gel electrophoresis and then dialyzed into storage buffer (100 mM phosphate pH 7.0, 100 mM NaCl, 10 mM β-mercaptoethanol, 50% glycerol). Protein concentrations were determined using molar extinction coefficients calculated from the amino acid sequence assuming denatured (6 M Guanidine HCl) or native conditions (*17*, *18*). The average values correspond to 18 000 M^{-1} cm^{-1} for *L. lactis* HisZ, 8300 $M^{-1}cm^{-1}$ for *L. lactis* HisG, 13 900 M^{-1} cm^{-1} for *B. subtilis* HisG, and 105 200 M^{-1} cm^{-1} for the *L. lactis* HisZG complex (a weighted average based on 4:4 stoichiometry).

Determination of Molecular Mass by Size Exclusion Chromatography and Laser Light Scattering. These experiments were carried out at the HHMI/W. M. Keck Foundation Biotechnology Resource Laboratory at Yale University. The system used for the analysis consisted of a size exclusion column (Superose 6, Pharmacia-Amersham) connected in tandem with three flow detectors: a UV detector (Model 773 variable wavelength, KRATOS, Applied Biosystems); a light scattering detector (DAWN DSP, Wyatt Technology); and a refractive index detector (OPTILAB, Wyatt technology). The solvent was delivered to the system by a Waters 510 pump (Waters Corp, Milford, MA) equipped with transducers to dampen pump pulsation, and a Rheodyne 7125 valve for sample injection. The buffer used for the analysis consisted of 100 mM Tris pH 8.1, 150 mM KCL, 10 mM $MgCl_2$, and 1 mM DTT. Prior to chromatography, samples were diluted 10-fold to reduce the glycerol content and then filtered through a 0.22 μm filter (Durapore, Millipore). The chromatography was performed at room temperature using

a flow rate of 0.4 mL/min. Standards for the analysis included apoferritin and bovine serum albumin.

In the size exclusion chromatography/laser light scattering (SEC-LS) technique, light scattering is proportional to the product of weight-averaged molecular mass and solute concentration. The relationship is given formally by eq 1, also described in ref *19*, which is based on the Rayleigh−Debeye−Gans light-scattering model that relates excess scattered light to concentration and weight-averaged molar mass moment (M_w) in grams per mole:

$$\frac{K^*c}{R(\theta)} = \frac{1}{M_w \times P(\theta)} + 2A_2c \quad (1)$$

In this equation, $R(\theta)$ is the excess of scattered light at angle θ, c is the sample concentration, M_w is the weight-averaged molecular weight (molar mass), and A_2 is the second virial coefficient. K^* is an optical parameter equal to the product $4\pi^2n^2(dn/dc)^2/(\lambda_0^4N_A)$ where n is the solvent refractive index, dn/dc is the refractive index increment, N_A is Avogadro's number, and λ_0 is the wavelength (cm) of the scattered light in a vacuum. $P(\theta)$ is a nonlinear function of the rms radius moment, r^2, a fitting method that might be advantageous for large random coil molecules. Several complementary methods are available to solve eq 1 for M_w and r^2. It is important to note that all the methods give nearly identical results for small molecules (rms radius less than 10 nanometers). Thus, any of the fitting formalisms can be used interchangeably for proteins with M_w less than 1×10^6 Da. Direct fitting of the data in this report using the Debeye method in the ASTRA software package allowed M_w to be determined. This fitting method is applicable over a wide range of molecular masses. More important, weight-averaged molecular weight determination is independent of the elution position of the protein, and is not influenced by nonglobular shape or interactions with the chromatography support.

Analytical Ultracentrifugation Experiments. All analytical ultracentrifugation experiments reported here were carried out at 20 °C in a Beckman XL-I analytical ultracentrifuge, equipped with an An50Ti rotor and both absorbance and interference optical detection systems. Purified proteins were stored at high concentration in 50% glycerol at −20 °C. Aliquots were dialyzed against a 2000-fold excess of AU buffer (50 mM Sodium Phosphate pH 7.5, 150 mM Sodium Chloride, 10 mM Magnesium Chloride) for 4−16 h at 4 °C using a Mini Dialysis Unit (Pierce) in order to reduce glycerol concentration prior to sedimentation studies. (Results from samples dialyzed 4 h did not significantly differ from those dialyzed overnight.)

Sedimentation velocity experiments on HisZ, HisG, or the HisZG ATP−PRTase complex were conducted at 50 000 rpm in a standard cell containing a two-sector Epon centerpiece and sapphire windows. Scans were collected using the interference mode and loading concentrations varied from 0.2 to 0.9 OD_{280}/mL, reflecting molar concentrations of about 7−70 μM, depending on the protein. Data from the sedimentation velocity experiments were analyzed using the boundary analysis method of van Holde and Weischet (*20*) and the time derivative of the concentration profile, $g(s^*)$, also called dC/dt (*21*). Both of these methods are implemented in the computer program UltraScan version 5 (*22*) running under the Slackware 7.1 distribution of the Linux computer operating system. Subroutines within Ultrascan also performed calculations for buffer density (ρ) and partial specific volume ($\bar{\nu}$) from the published protein sequences of HisZ and HisG (*9*). The calculated $\bar{\nu}$ of *L. lactis* HisZ, *B. subtilis* HisG, and *L. lactis* HisG were 0.7381, 0.7396, and 0.7503 cm^3/g, respectively. The weighted $\bar{\nu}$ values for the 4:4 and 2:6 models of the HisZG ATP−PRTase complex were 0.7415 and 0.7439 cm^3/g, respectively. The sedimentation coefficient is directly proportional to the effective molar mass of the particle (corrected for its buoyancy), inversely proportional to the frictional coefficient, and is independent of the other operating conditions. Measurements are reported in units of Svedbergs, S, and have been further corrected for solvent density and viscosity relative to that of water at 20 °C ($S^0_{20,w}$, where 1 S = 10^{-13} s). In the van Holde Weischet method the S values are extrapolated to infinite sedimentation time which removes uncertainties in S that arise from the effects of diffusion.

Sedimentation equilibrium experiments on HisZ and HisG were analyzed in AU buffer with six sector centerpieces allowing up to three different protein concentrations to be analyzed in one experiment. As determined by Coomassie stained SDS−PAGE gels, each protein was stable over the course of a 72 h experiment (data not shown). Absorbance at 280 nm was measured as a function of radial position for three rotor speeds, ranging from 16 000 to 33 000 rpm. Equilibrium at each rotor speed was considered to be reached when scans separated by 4 h or longer were indistinguishable. At that time, five scans were averaged for each sample at each rotor speed. The sedimentation properties of independently expressed and purified HisZ or HisG were analyzed with MacNonlin-PPC, fitting to a model which describes the sedimentation of homogeneous, ideal monomers:

$$C_r = C_{r0}\{\exp[(\omega^2/2RT)M(1 - \bar{\nu}\rho)(r^2 - r_0^2)]\} + \Delta E \quad (2)$$

where C_r is the concentration at radius r, C_{r0} is the concentration of the monomer at the reference radius r_0, ω is the angular velocity, R is the gas constant, T is temperature in Kelvin, M is the monomer molecular weight, $\bar{\nu}$ is the partial specific volume of the solute, and ρ is the density of the solvent. ΔE is the baseline offset parameter used in fitting.

The equation used for fitting to a monomer dimer model was

$$C_{total} = C_{monomer,r0}\{\exp[(\omega^2/2RT)M(1 - \bar{\nu}\rho)(r^2 - r_0^2)]\} + C_{n-mer,r0}\{\exp[(\omega^2/2RT)2M(1 - \bar{\nu}\rho)(r^2 - r_0^2)]\} + \Delta E \quad (3)$$

Association constants were calculated by converting K_{abs} returned from the fitting routine, into molar concentration units using a modified form of the Beer−Lambert Law:

$$K_{assoc} = (K_{abs} \times \epsilon^{n-1} \times L^{n-1}) \div n \quad (4)$$

where ϵ = molar extinction coefficient (listed above), L = path length (1.2 cm in the ultracentrifuge), and n = association state modeled (dimer = 2).

RESULTS

Purification of the Transferase−Separation of the HisZ and HisZG Subunits by Size Exclusion and Hydroxyapatite

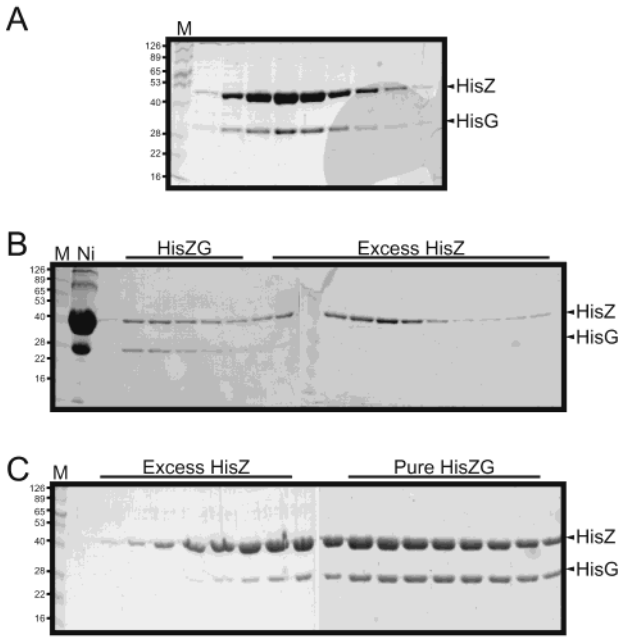

FIGURE 1: Purification of the HisZG ATP−PRTase complex. (A) Co-purification by affinity chromatograpy on Ni−NTA agarose. (B) Separation of HisZG from excess HisZ by size exclusion chromatography on Superdex 200. (C) Hydroxyapatite chromatography. A molecular weight standard lane, M, is indicated at left. The mobilities of HisZ and HisG are denoted by arrowheads. Lane Ni shows the pool from step A that was applied to Superdex 200.

Chromatography. A multistep purification scheme was developed to separate free HisZ from the HisZG complex, allowing the complex to be characterized in detail. This scheme comprises Ni−NTA chromatography, Superdex 200 size exclusion chromatography, and hydroxyapatite chromatography. As shown in Figure 1, use of the Superdex 200 column followed by subsequent hydroxyapatite chromatography permitted separation of the HisZG complex from free HisZ. For comparative purposes, stocks of the isolated HisZ from *L. lactis* and HisG from *Bacillis subtilis* were also prepared. The choice of HisG from *B. subtilis* as opposed to *L. lactis* was predicated on the observation that the expression level of *L. lactis* HisG in *E. coli* was much less than the *B. subtilis* enzyme. On the basis of the 44% identity (90/203 residues) between HisG from these two organisms, the two proteins are assumed to behave identically with respect to their biochemistry.

Hydrodynamic Analysis of Isolated HisZ and HisG Components. Investigation of the stoichiometry of the *Lactococcus lactis* HisZG enzyme was initiated by an examination of the hydrodynamic properties of the independently purified polypeptides. Preliminary sedimentation velocity experiments were carried out on *L. lactis* HisZ or *B. subtilis* HisG under physiological pH and salt concentrations, using protein concentrations close to those employed in the SEC-LS experiments described below. In isolation, HisZ and HisG sedimented as monodisperse species at 4.1 and 3.4 S, respectively, indicating that the overexpressed proteins were stable, with no significant concentration dependent nonideality under experimental conditions (data not shown).

Both proteins were therefore good candidates for sedimentation equilibrium studies, allowing molecular masses, association constants, and stoichiometries to be determined. Each protein was centrifuged to equilibrium at three speeds

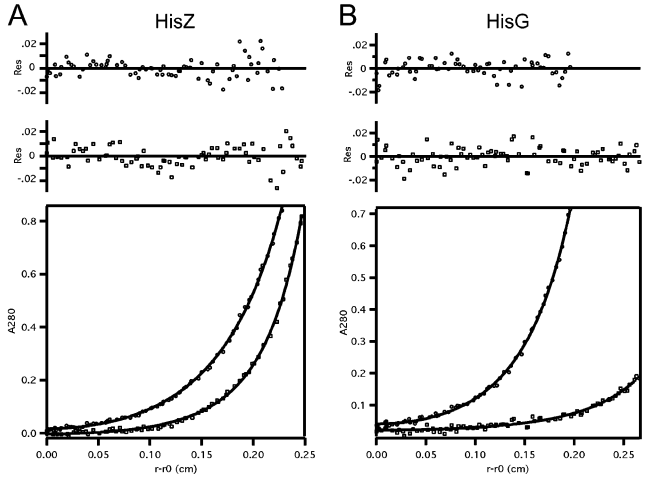

FIGURE 2: Sedimentation equilibrium characterization of independently expressed and purified HisZ and HisG. Representative examples of at least four scans at equilibrium for different rotor speeds and initial loading concentrations were globally fit to determine association state and solution molecular mass of HisZ and HisG. Solid lines represent global fits of the monomer−dimer model (eq 3) to the data sets obtained. Fits returned M_r values of 72 340 ± 5350 for HisZ and 48 276 ± 4400 for HisG. In both cases the residuals of the fits (Res) were small and symmetrically distributed.

and three initial loading concentrations, resulting in four to six data sets for each protein that were subjected to global fitting. Figure 2 shows representative individual scans with fitted curves and residuals for both HisZ and HisG. The equilibrium concentration distributions for each protein were well described by global fits to a monomer−dimer model, providing strong evidence for dimer formation in solution. The molecular masses returned were 72 340 ± 5350 for $(HisZ)_2$ and 48 276 ± 4400 for $(HisG)_2$. The association constants calculated for HisZ and HisG were 8.4×10^5 and 2.3×10^5 M^{-1}, respectively, indicating that the majority of isolated HisZ and HisG are dimers in solution when the concentration is greater than 1 μM. Fits to other models including monomer-trimer, monomer−dimer-hexamer, or monomer−dimer−tetramer returned poor thermodynamic and statistical values (data not shown). These experiments suggest that the large HisZ−HisG complex is assembled from dimers of the HisZ and HisG component species.

Determination of Molecular Weight by SEC-LS. As a first approach to determine the solution molecular mass of the higher order HisZG enzyme complex, size exclusion chromatography coupled with continuous measurement of laser light scatter and refractive index of the eluted sample was employed. This technique can provide accurate (±5%) solution molecular weight determination that is independent of the SEC elution position, does not require modification of the protein, and can be used under a wide variety of solution conditions (*19*). A sample of HisZG complex purified through the Superdex 200 step produced two peaks during analytical gel filtration, a major peak eluting at 15.2 mL and a minor peak eluting at 16.4 mL (Figure 3, Table 1). On the basis of the Debeye fitting method, the major peak contained macromolecules with a molecular mass range of 172−224 kDa and a weight-averaged molecular mass of 213 kDa for the entire peak (Table 1). This molecular mass is indicative of a complex that likely includes multiple subunits of HisZ and HisG. The pronounced asymmetry of

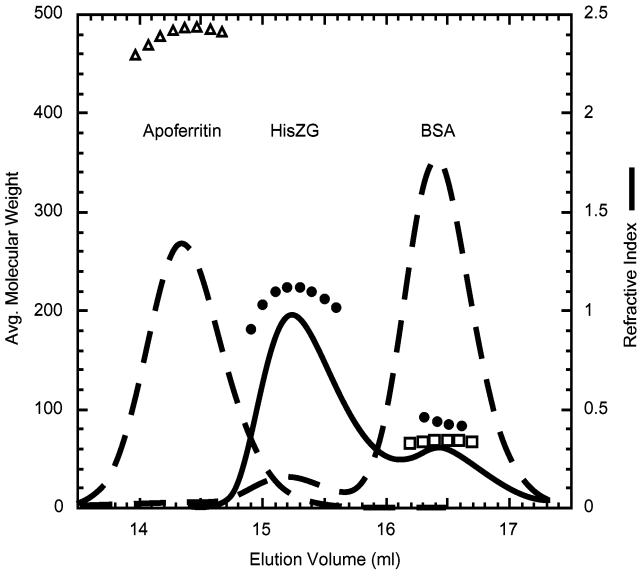

FIGURE 3: Estimation of the molecular mass of HisZG by HPLC−SEC/LS. The experimental protocol is described in the Materials and Methods. Symbols indicate weight-averaged molecular mass read from the left ordinate for apoferritin (triangle), HisZG (circle), and bovine serum albumin (BSA, square). Solid lines show the HisZG refractive index profile read from the right ordinate. Two reference protein standards (broken lines) were analyzed independently, and the results are superimposed in this figure. All proteins were examined under the same set of conditions.

Table 1: Results of SEC-LS Analysis of *Lactococcus lactis* HisZG ATP−PRTase[a]

elution peak[b] (mL)	average M_w[c] (kDa)	M_w range[d] (kDa)	polydisperse[e] (yes/no)
15.2	213	172−224	yes
16.4	85	79−94	yes

[a] Analysis was performed as described in the Materials and Methods by the Biotechnology Resource Laboratory at Yale University. [b] A peak is defined as the elution point of a UV absorption trace maximum. [c] Weight-averaged molar mass moments were calculated in 1 s increments using the ASTRA software package. [d] M_w range reflects the lowest and highest average MW determined for the selected peak areas. [e] Polydispersity was calculated as weight-averaged molar mass divided by number-averaged molar mass and was greater than unity for both peaks.

the major peak and the substantial 30% variability in the molecular mass range, which followed the concentration profile, suggest a dynamic equilibrium among heterogeneous multimeric states. By contrast, control proteins apoferritin (476 kDa 24-mer) and bovine serum albumin (66 kDa) exhibited symmetrical peaks with variations in weight-averaged molecular mass of less than 5%. The minor peak of the HisZ−HisG complex had a molecular mass range between 79 and 94, with a weight average of 85 kDa, which constituted a 19% variability over the indicated range. However, the weight-averaged molecular mass became stable at about 80 kDa after 16.5 mL elution, implying a predominant species with this molecular mass.

A likely explanation for these observations is that the complex eluting at 15.2 mL is in equilibrium with potential intermediate assembly states (including free HisZ and/or HisG dimers) eluting at 16.4 mL. An important consequence of the proposed equilibrium between the two main populations in this sample is that it may lead to an apparent underestimation of the molecular masses of the HisZ−HisG complex estimated by the use of the Debeye plot (*19*). A comparison of candidate species on the basis of their predicted molecular weights from amino acid composition in relation to the results obtained from SEC-LS is shown in Table 2. The observed mass of 224 kDa associated with the major peak can be accounted for by either of two putative octamers, $HisZ_2HisG_6$ and $HisZ_4HisG_4$, which have predicted M_r's of 222 620 and 249 640, respectively. The minor peak, whose maximum mass from the Debeye plot was 94 kDa, can be modeled by at least four complexes whose predicted masses are close to this value, but not less (Table 2). Three of these represent possible dimer-pair intermediates in the formation of an octameric complex. The fourth possibility consists of a trimer containing two HisZ subunits and one HisG subunit. While the mass of this species is closer to the weight-averaged mass than the heterotetramer $HisZ_2HisG_2$, it represents an unlikely dissociation species, because it involves a subcomplex with a single subunit of HisG.

Table 2: Comparison of M_w Estimates from SEC-LS and Amino Acid Sequence

subunit composition[a]	average M_w of selected peak[b]	predicted M_w[c]
$HisZ_4$ $HisG_4$	213 000	249 640
$HisZ_2$ $HisG_6$	213 000	222 620
$HisZ_2$ $HisG_2$	85 000	124 820
$HisZ_2G$	85 000	100 370
$HisZ_4$	85 000	151 840
$HisG_4$	85 000	97 800

[a] Putative assembly states were selected on the basis of expected molecular mass. [b] Data taken from Table 1. [c] Values were calculated from the known amino acid sequences of *L. lactis* HisZ and HisG.

Hydrodynamic Analysis of the Complete HisZG ATP−PRTase. The above results suggested that the complex is predominantly a single population composed of multiples of HisZ and HisG dimers, but provided little information about the stoichiometry of the complex or the strength of association. Sedimentation velocity analysis was performed on the complex to address these questions and probe the effects of substrates or inhibitors on complex stability. Preliminary experiments using HisZG purified through the gel filtration step detected two populations of macromolecules (as in the SEC-LS studies) which sedimented at about 5 and 10 S (data not shown). When a more homogeneous HisZG preparation (purified through the hydroxyapatite column) was used, the majority of the material sedimented at 10.1 S, and the 5 S material disappeared (Figure 4). The 5 S peak may therefore correspond to excess HisZ dimers carried over during early steps in the purification.

Substrate Binding Effects on Macromolecular Assembly of HisZG. Sedimentation velocity experiments can be informative about heterogeneity within a sample of sedimenting macromolecules, and such heterogeneity can often be attributed to different associated species or different conformations of the same macromolecule or both. In light of the reported changes in the sedimentation behavior of the homohexameric HisG in response to substrates and inhibitors, it was of interest to determine whether similar changes occur for the heteromeric enzyme. Four ligands were tested in combination with the HisZG enzyme. These included ATP and PRPP, the substrates required for the ATP−PRTase reaction, and histidine and AMP, inhibitors of the hexameric

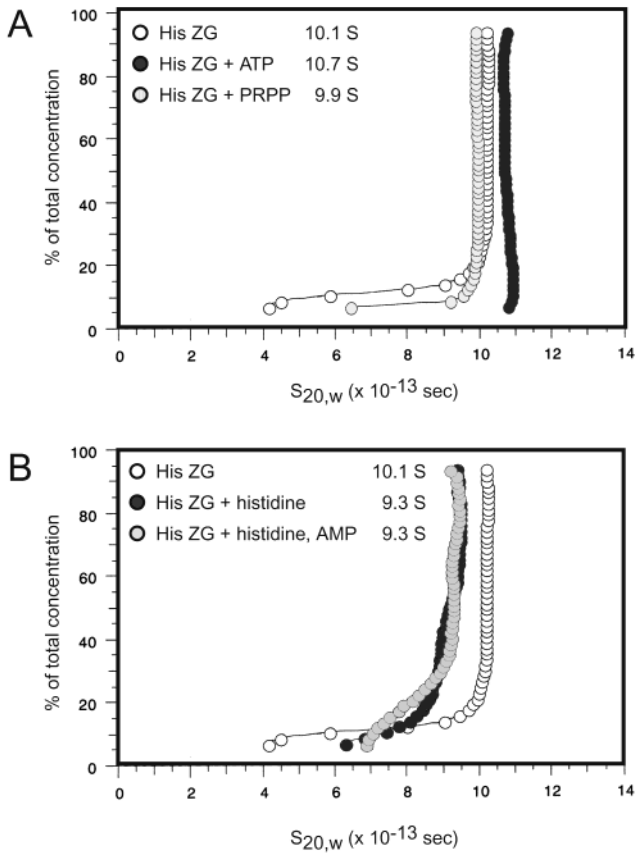

FIGURE 4: Sedimentation velocity analysis of HisZG ATP−PRTase from *L. lactis* in the presence of substrates and inhibitors. Data were collected on the enzyme complex alone or in the presence of various ligands. vanHolde Weischet integral distribution plots are shown. (A) Unliganded HisZG (open symbols) and HisZG + 1 mM ATP or 0.2 mM PRPP (black and gray symbols). (B) Unliganded HisZG (open symbols) and HisZG + 1 mM histidine, or 1 mM histidine and 0.75 mM AMP (black and gray symbols). Each data point represents approximately 2% of the total protein concentration. Sedimentation coefficients listed were calculated for the total protein concentration shown.

enzyme (*3*, *23*). The results are summarized in vanHolde Weischet distribution plots (Figure 4) which show the integral distribution of *S* values in the sample over the total concentration range of the sedimentation boundary. As shown by the vertical distribution, the unliganded complex is homogeneous, and virtually all material sediments at 10.1 S (Figure 4A and 4B, open symbols). The amount of material sedimenting at smaller *S* values was less than 10%. This latter observation is not surprising, as the concentration of HisZG in these experiments was within three to five times the dissociation constants estimated for HisZ and HisG dimers. Accordingly, a small fraction of HisZ and HisG monomers and dimers would be expected to be in equilibrium with the large complex. When the substrates ATP and PRPP were added separately (Figure 4A) the distribution of *S* values became even more homogeneous, which may be interpreted as a modest stabilization of the complex. However, the more notable result was an increase in *S* of the complex from 10.1 to 10.7 S in the presence of ATP, but not PRPP. Such a change is consistent with a conformational change that increases the sedimentation rate of the ATP-bound complex. By contrast, the presence of histidine or AMP plus histidine caused a decrease in the sedimentation rate of the complex

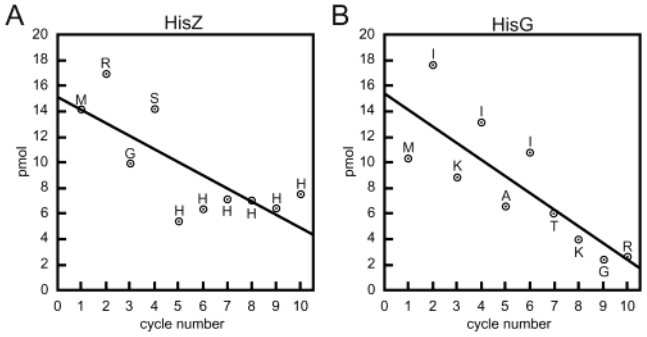

FIGURE 5: Quantitative protein sequencing of the purified HisZG ATP−PRTase. HisZ and HisG present in a sample of the purified HisZG complex were separated by denaturation and fractionation on SDS−PAGE and then electroblotted onto PVDF membrane. Ten cycles of N-terminal sequencing were performed on excised HisZ or HisG. The repetitive yields for each cycle were calculated and were plotted vs cycle number. Solid lines represent linear least-squares fits where $R^2 = 0.56$ and 0.66 for HisZ and HisG, respectively. Extrapolation to the *Y*-axis (cycle 0) gives the total yield for each protein, in picomoles.

to 9.3 S, with at least 40% of the total protein in an equilibrium between 7 and 9 S (Figure 4B). This decrease in the velocity of sedimentation from 10.1 to 9.3 S was largely driven by histidine, while AMP influenced the relative distribution of protein at the slower *S* values.

Collectively, these results indicate that, depending on the ligands present, the intact and functional form of the HisZG ATP−PRTase is a complex that sediments between 9.3 and 10.7 S. The stability and homogeneity of the complex is apparently increased by the substrates ATP and PRPP but decreased in the presence of the regulatory inhibitor histidine. These results provide the first evidence that the heteromeric HisZG enzyme undergoes some type of global structural change in response to substrate or inhibitor binding.

Determination of Overall Subunit Stoichiometry by Quantitative Protein Sequencing. One issue left unresolved by the SEC-LS or the analytical ultracentrifuge experiments is the stoichiometric ratio of HisZ and HisG in the complex, a parameter useful in choosing between possible octameric models of the complex. To provide a more definitive estimate of the overall HisZ to HisG ratio, quantitative protein sequencing was performed. The two octameric models of the HisZG complex predict different ratios of the two polypeptide chains: a 1:3 ratio in the case of the $HisZ_2HisG_6$ model and a 1:1 ratio in the case of the $HisZ_4HisG_4$ complex. A sample of the complex purified through all three chromatography steps was subjected to denaturing polyacrylamide gel electrophoresis and then transferred to PVDF membrane to allow N-terminal sequencing by the Edman method. Liberated amino acid at each of 10 protein sequencing steps was quantified and then plotted against cycle number to provide an estimate of total protein before sequencing (Figure 5). On the basis of this analysis, the extrapolated quantity of each polypeptide was close to 15 pmol. Even when the less robust fitting of HisZ is taken into account, the data strongly suggest that the HisZ and HisG polypeptides are present in equimolar amounts. Thus, the $HisZ_2HisG_6$ model for the octameric complex can be ruled out, suggesting that the true complex stoichiometry is most likely to be $HisZ_4HisG_4$.

DISCUSSION

HisZ−HisG ATP PRTase is an Octamer in Equilibrium with a Tetrameric Species. In this study, a variety of approaches were used to address the aggregation state of the "short form" HisG ATP−PRTase. Unlike the "long form" HisG enzymes, which are hexamers composed of identical subunits, the short form HisG enzyme is actually a heteromeric complex. The results presented here suggest that the HisZG ATP−PRTase is best modeled as a complex that contains eight polypeptide chains, with an equimolar stoichiometry of HisZ and HisG. While SEC-LS and preliminary sedimentation velocity experiments both indicated that preparations of the heteromeric complex contained two predominant species, the majority of the material analyzed by SEC-LS behaved as a complex with a molecular mass near 224 kDa. This is compatible with models described by $HisZ_2HisG_6$ or $HisZ_4HisG_4$ complexes. Quantitative protein sequencing confirmed that both polypeptides are present in equimolar amounts, indicating that the $HisZ_4HisG_4$ complex represents the most likely association state of the intact complex. This proposed octameric structural model is unique among both the aminoacyl-tRNA synthetases and the PRTases.

The precise determination of molecular weight of the complex was initially hampered by its size heterogeneity in SEC-LS and initial sedimentation velocity experiments. This problem was solved for the remainder of sedimentation velocity experiments on HisZG by excluding from the purification scheme chromatography fractions found to retain a significant excess of HisZ over HisG. The 5 S species seen in the early sedimentation studies was eliminated by this modification, suggesting that it represented excess HisZ dimers in exchange with those in the octameric complex. Such a conclusion is strongly supported by the fact that the weight-averaged M_w for the latter half of the small peak from SEC-LS was stable at about 80 kDa, the correct value for a HisZ dimer.

In contrast to the numerous lines of evidence for two dimers of each polypeptide in the 10.1 S complex, there was less evidence for assembly intermediates, which could include a $HisZ_2HisG_2$ tetramer or $HisG_6$ hexamer. Homotetrameric species of the types listed in Table 2 seem unlikely on the basis of their absence in sedimentation equilibrium studies above. Nevertheless, the possible existence of a heterotetramer of one HisZ and one HisG dimer has not been ruled out and was suggested by MALDI-TOF mass spectroscopy analysis. While no peaks corresponding to the intact octamer or homotetramers were observed in the spectra, a small but distinct peak with *m*/*z* equal to 119 002 was observed (data not shown). This lies within 1.5% of the combined mass of one HisZ and one HisG dimer ($HisZ_2$-$HisG_2$) from the sedimentation equilibrium experiments. The remaining peaks were consistent with dimeric and monomeric forms of HisZ and HisG (data not shown). Considering the results summarized above, our current working model (Figure 6) suggests the octameric transferase is assembled from dimers of HisZ and HisG, perhaps with the involvement of a putative heterotetrameric intermediate. Further studies will be necessary to determine whether this putative tetramer assembly intermediate has any physical or biological relevance.

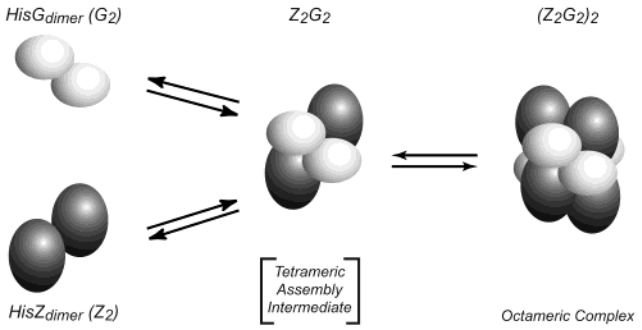

FIGURE 6: Model of complex formation for the HisZG ATP−PRTase. Dimers of HisZ and HisG are represented as oblate spheres. The reversible association of dimers to tetramer and tetramer to octamer is indicated by double-headed arrows. In the absence of experimental data concerning symmetry relationships between the HisZ and HisG protomers, the configuration shown represents but one of many possible subunit arrangements in the functional complex.

Allosteric Modulation of HisZG Structure by Substrates and Inhibitors. Among the most notable observations of our studies are the changes in sedimentation properties of HisZG in response to substrates and inhibitors. First, ATP increased the homogeneity of HisZG with respect to sedimentation behavior and shifted the complex to a faster *S* value of 10.7, while the inhibitors histidine and AMP resulted in a range of S in equilibrium from 7 to 9.3 S. These changes in sedimentation behavior may be attributable to conformational changes of HisZG in the presence of ligands and, additionally or alternatively, changes in subunit composition. In at least two other systems, aspartate transcarbamoylase and glycogen phosphorylase, changes in sedimentation behavior upon substrate or inhibitor binding have been interpreted as representing bona fide allosteric transitions (*24*, *25*). Moreover, comparison of the structures of unliganded HisRS and its histidine-bound complex indicate a substantial conformational change involving the insertion domain and other structural elements (*26*, *27*). Thus, the precedent for at least the HisZ subunit undergoing conformational changes in response to histidine binding is well established. The molecular basis of an ATP induced comformational change is less clear, but could additionally involve a shift in the equilibrium from smaller subunit species to an active octameric complex. In this context, we note that the HisZG ATP−PRTase catalytic velocity exhibits a sigmoidal dependence on ATP concentration (K. Champagne, M. Sissler, CSF, manuscript in preparation) possibly indicating ATP-induced stabilization of the active octameric complex.

Comparison of the Octameric and Hexameric ATP−PRTases. The imprecision in the mass estimates for the substrate free octamer reported here are reminiscent of the behavior of the "long forms" of HisG found in the enteric bacteria, both of which were reported to be nominal hexamers. As in the case of the heteromeric HisZG, the homohexamer of HisG from enteric bacteria shows altered sedimentation behavior in response to substrates, inhibitors, and other experimental conditions (*3*, *4*). For the *S. typhimurium* enzyme, the hexamer form was observed to predominate for freshly prepared enzyme under standard assay condition, namely, pH 7.5−8.5, 100 mM sodium chloride, and 22−37 °C (*3*). However, conditions of low enzyme concentration and elevated pH (e.g., pH 10) pro-

moted the dissociation of the enzyme into dimers, while elevated temperatures and high salt conditions promoted aggregation to a species greater than the hexamer. Despite this behavior under altered conditions, active enzyme−substrate sedimentation velocity experiments provided evidence that the physiologically active species is a hexamer. Thus, Parsons and Koshland concluded that, despite variations in oligomerization conditions, the likely physiologically important form of the enzyme is a hexamer (*3*).

Opposite conclusions were drawn from similar studies carried out on the *E. coli* ATP−PRTase. The *E. coli* enzyme exhibited considerable polydispersity in gel filtration experiments, and the presence of substrates and products altered the preferred association state, with PRPP stabilizing the dimeric form of the enzyme (*4*, *28*). In reviewing these data and other relevent studies (*29*, *30*), Dall-Larsen (*16*) concluded that the active form of the *E. coli* enzyme is a dimer, with the inhibitors histidine and AMP (as well as the product, PR−ATP) bringing about association of dimers into an inactive hexamer. More recently, crystals of *E. coli* HisG were described with space group *R*32, consistent with a hexameric asymmetric unit possessing both 2-fold and 3-fold axes of symmetry (*31*). Owing to the high sequence similiarity between HisG from *S. typhimurium* and *E. coli*, it is implausible to imagine that the active forms of the two enzymes possess different oligomeric states. Additional structural studies of the hexameric form will be required to resolve these discrepancies. Nevertheless, these prior studies emphasize that, despite differences in subunit stoichiometry and molecular mass of the quaternary complexes, the hexameric HisG and octameric HisZ−HisG enzymes are both likely to undergo significant structural changes in response to inhibitor (and perhaps substrate) binding.

Comparison of the long and short forms of HisG suggests that the differences in oligomeric structure are not likely to be due to differences in the catalytic portion of HisG. The sequences of *L. lactis* and *E. coli* HisG are 40% identical over the first 200 amino acids, suggesting that the conserved portions of the protein are unlikely to dictate the oligomeric structure. However, limited proteolysis studies on HisG from *L. lactis* indicate that elements within the first 50 amino acids are necessary for interaction with HisZ (M. Sissler and C. S. F., unpublished data, 2000). Thus, there are likely to be at least two different regions in *L. lactis* HisG that are important for quaternary interactions, the first stabilizing the HisG dimer and the second promoting interactions with HisZ. The C-terminal 100 amino acids absent in the short form are likely to be required for specifying the hexameric structure of the long form, a structural function replaced by HisZ in the octameric form of the transferase. To carry out this function, HisZ must possess both a homodimeric interface, and an heterodimeric interface with HisG. However, sequence comparisons between HisZ and functional histidyl-tRNA synthetases suggest no obvious regions that might be required for contact with HisG.

Comparison with Other PRTase Families. The unusual hexameric and octameric quaternary structures of the ATP−PRTases are rare among the PRTases, which are typically dimers or tetramers (*32*). Sequence and structural comparison of this superfamily suggests that it comprises at least three unrelated structural families. The type I enzymes, which include hypoxanthine PRTase, adenine PRTases, orotate PRTases, and glutamine amidotransferases (GPATs), are based on a parallel β-sheet catalytic fold flanked by α-helices; substrates are bound via loops that protrude from the C-terminal edge of the sheet (*13*). Type I enzymes are further distinguished by an 11-amino-acid PRPP binding motif that includes catalytic residues contributed by one of the active site loops. A second group, the type II enzymes, are described by a sole family, the quinolate PRTases (QPRTase) (*14*). The QPRTase is an obligate dimer composed of an N-terminal domain based on a four-stranded open β sandwich and a C-terminal α/β domain comprising seven of the eight strands of an α/β TIM barrel. The active site is located in the interface between these two domains. A third family based on an unrelated parallel β-sheet fold was recently reported for CobT, a PRTase involved in the synthesis of α-ribazole, a molecule that serves as part of the lower ligand of cobalamin (*15*). Significantly, there is no identifiable sequence similarity between the PRTases of known structure classified in the three subfamilies and the ATP−PRTases. Yet structural similarities between HisG and the other PRTase families might emerge when the structures of the octameric and hexameric ATP−PRTases are determined.

Despite the absence of detectable homology at the level of amino acid sequence, there is an important functional similarity between the ATP−PRTases and the glutamine amidotransferase PRTases (GPAT). The GPATs catalyze the first committed step of purine synthesis, a reaction in which the amino group of glutamine is transferred to PRPP to form phosphoribosyl-1-amine (*33*). The activity of GPAT is regulated by purine nucleoside monophosphates, which serve as allosteric inhibitors. These PRTases are two domain enzymes, the first of which provides NH_3^+ by hydrolysis of glutamine, while the second catalyzes the phosphoribosyl transferase reaction (*34*). This second domain is approximately the same size as the short form HisG polypeptide. As determined from various crystal structures, the GPATs from a number of different sources are tetramers (*34*−*36*). In solution, however, the GPAT tetramer is in equilibrium with dimers and monomers (*37*). Thus, the ATP−PRTases and GPATs constitute two of the most complex allosterically regulated PRTases and exhibit similar solution behavior with respect to their quaternary structures. Further structural studies of the ATP PRTases are likely to reveal whether there are other important similarities between these two important families of phosphoribosyl transferases.

ACKNOWLEDGMENT

We gratefully acknowledge the assistance of Ewa Folta-Stogniew at the HHMI Biopolymer Laboratory & W. M. Keck Foundation Biotechnology Resource Laboratory at Yale University for collecting and analyzing the SEC-LS data and Stephen Smith, M.S. at the University of Texas Medical Branch Protein Chemistry Laboratory (Galveston, TX), for providing peptide sequencing analyses. We also thank Dr. Mark E. Rogers and Christopher D. Ziegenfuss, B.S. at M-Scan Inc. (West Chester, PA), for performing the mass spectral analysis.

REFERENCES

1. Voll, M. J., Appella, E., and Martin, R. G. (1967) *J. Biol. Chem. 242*, 1760−7.

2. Carlomagno, M. S., Chiariotti, L., Alifano, P., Nappo, A. G., and Bruni, C. B. (1988) *J. Mol. Biol. 203*, 585−606.
3. Parsons, S. M., and Koshland, D. E., Jr. (1974) *J. Biol. Chem. 249*, 4119−26.
4. Klungsoyr, L., and Kryvi, H. (1971) *Biochim. Biophys. Acta 227*, 327−36.
5. Winkler, M. E. (1987) in *Escherichia coli and Salmonella Typhimurium. Cellular and Molecular Biology* (Neidhardt, F. C., Ed.) pp 395−411, American Society for Microbiology, Washington, DC.
6. Alifano, P., Fani, R., Lio, P., Lazcano, A., Bazzicalupo, M., Carlomagno, M. S., and Bruni, C. B. (1996) *Microbiol. Rev. 60*, 44−69.
7. Mori, I., Fonne-Pfister, R., Matsunaga, S., Tada, S., Kimura, Y., Iwasaki, G., Mano, J., Hatano, M., Nakano, T., Koizumi, S., Scheidegger, A., Hayakawa, K., and Ohta, D. (1995) *Plant Physiol. 107*, 719−723.
8. Sissler, M., Delorme, C., Bond, J., Ehrlich, S. D., Renault, P., and Francklyn, C. (1999) *Proc. Natl. Acad. Sci. U.S.A. 96*, 8985−90.
9. Delorme, C., Ehrlich, S. D., and Renault, P. (1992) *J. Bacteriol. 174*, 6571−9.
10. Kunst, F., Ogasawara, N., Moszer, I., Albertini, A. M., Alloni, G., Azevedo, V., Bertero, M. G., Bessieres, P., Bolotin, A., Borchert, S., Borriss, R., Boursier, L., Brans, A., Braun, M., Brignell, S. C., Bron, S., Brouillet, S., Bruschi, C. V., Caldwell, B., Capuano, V., Carter, N. M., Choi, S. K., Codani, J. J., Connerton, I. F., Danchin, A., et al. (1997) *Nature 390*, 249−56.
11. Eriani, G., Delarue, M., Poch, O., Gangloff, J., and Moras, D. (1990) *Nature 347*, 203−206.
12. Bond, J. P., and Francklyn, C. (2000) *J. Mol. Evol. 50*, 339−47.
13. Smith, J. L. (1999) *Nat. Struct. Biol. 6*, 502−4.
14. Eads, J. C., Ozturk, D., Wexler, T. B., Grubmeyer, C., and Sacchettini, J. C. (1997) *Structure 5*, 47−58.
15. Cheong, C. G., Escalante-Semerena, J. C., and Rayment, I. (1999) *Biochemistry 38*, 16125−35.
16. Dall-Larsen, T. (1988) *Int. J. Biochem. 20*, 231−5.
17. Gill, S. C., and von Hippel, P., H. (1989) *Anal. Biochem. 182*, 319−326.
18. Pace, C. N., Vajdos, F., Fee, L., Grimsley, G., and Gray, T. (1995) *Protein Sci. 4*, 2411−23.
19. Folta-Stogniew, E., and Williams, K. R. (1999) *J. Biomol. Techniques 10*, 51−63.
20. van Holde, K. E., and Weischet, W. O. (1978) *Biopolymers 17*, 1387.
21. Stafford, W. F., 3rd. (1992) *Anal. Biochem 203*, 295−301.
22. Demeler, B. (2001) *Ultra Scan 5.0 − Ultracentrifugation Data Analysis Software*, University of Texas Health Science Center, San Antonio, TX (http://www.ultrascan.uthscsa.edu).
23. Blasi, F., Aloj, S. M., and Goldberger, R. F. (1971) *Biochemistry 10*, 1409−17.
24. Eisenstein, E., Markby, D. W., and Schachman, H. K. (1990) *Biochemistry 29*, 3724−31.
25. Oikonomakos, N. G., Kontou, M., Zographos, S. E., Watson, K. A., Johnson, L. N., Bichard, C. J., Fleet, G. W., and Acharya, K. R. (1995) *Protein Sci. 4*, 2469−77.
26. Qiu, X., Janson, C. A., Blackburn, M. N., Chhohan, I. K., Hibbs, M., and Abdel-Meguid, S. S. (1999) *Biochemistry 38*, 12296−304.
27. Yaremchuk, A., Tukalo, M., Grotli, M., and Cusack, S. (2001) *J. Mol. Biol. 309*, 989−1002.
28. Tebar, A. R., Fernandez, V. M., Martin Del Rio, R., and Ballesteros, A. O. (1973) *Experientia 29*, 1477−9.
29. Tebar, A. R., and Ballesteros, A. O. (1976) *Mol. Cell Biochem. 11*, 131−6.
30. Dall-Larsen, T. (1988) *Int. J. Biochem. 20*, 811−5.
31. Lohkamp, B., Coggins, J. R., and Lapthorn, A. J. (2000) *Acta Crystallogr., Sect. D: Biol. Crystallogr. 56*, 1488−91.
32. Musick, W. D. (1981) *CRC Crit. Rev. Biochem. 11*, 1−34.
33. Zalkin, H., and Smith, J. L. (1998) *Adv. Enzymol. Relat. Areas Mol. Biol. 72*, 87−144.
34. Smith, J. L., Zaluzec, E. J., Wery, J. P., Niu, L., Switzer, R. L., Zalkin, H., and Satow, Y. (1994) *Science 264*, 1427−33.
35. Muchmore, C. R., Krahn, J. M., Kim, J. H., Zalkin, H., and Smith, J. L. (1998) *Protein Sci. 7*, 39−51.
36. Krahn, J. M., Kim, J. H., Burns, M. R., Parry, R. J., Zalkin, H., and Smith, J. L. (1997) *Biochemistry 36*, 11061−8.
37. Wong, J. Y., Bernlohr, D. A., Turnbough, C. L., and Switzer, R. L. (1981) *Biochemistry 20*, 5669−74.

BI020243Z